In-situ quantification of ice rheology and direct measurement of the Raymond Effect at Summit, Greenland using a phase-sensitive radar

Fabien Gillet-Chaulet,[1,2] Richard C. A. Hindmarsh,[2] Hugh F. J. Corr,[2] Edward C. King,[2] and Adrian Jenkins[2]

[1]   The Glen exponent n characterizes the stress-dependence of ice deformation, directly influencing the rate at which ice masses respond to external forcing. The slow deformation in large ice-sheets makes laboratory rheometry at representative strain-rates difficult. We develop a new technique to estimate n in-situ, deploying a phase-sensitive radar to measure vertical strain rates of around 10^{-4} yr^{-1} within the top 1000 m of ice across ice divides at Summit and NEEM, Greenland. A fluid-dynamical feature, the Raymond Effect, predicts strong vertical strain-rate variation across divides over distances of a few ice-thicknesses. We achieve sufficient resolution to show this pattern, enabling us to estimate $n = 4.5$ by inverting our observations with flow modelling. This is higher than values previously used but consistent with other indirect measurements, implying laboratory measurements do not explore the full range of ice rheology and the consequent possibility of a greater sensitivity and responsiveness in ice-sheet dynamics. **Citation:** Gillet-Chaulet, F., R. C. A. Hindmarsh, H. F. J. Corr, E. C. King, and A. Jenkins (2011), In-situ quantification of ice rheology and direct measurement of the Raymond Effect at Summit, Greenland using a phase-sensitive radar, *Geophys. Res. Lett.*, *38*, L24503, doi:10.1029/2011GL049843.

1.   Introduction

[2] In recent years, the quality and quantity of data describing ice-sheet geometry and motion has increased considerably, so that our ability to describe the current state of the ice-sheets is no longer the limiting factor in making predictions. Despite this progress, the in-situ rheology of ice, which determines the rate at which the ice can flow and respond to external changes is still poorly understood and constrained. Uncertainties in the processes that govern the deformation of ice arise from the fact that in-situ strain-rates are not reproducible in laboratories, while field measurements are difficult to devise owing to the difficulties in completely characterising the strain-rate and stress tensors.

[3] For ice flowing according to a non-linear Glen rheology, *Raymond* [1983] predicted the presence of a nearly-stagnant plug of stiff ice under ice divides, inducing horizontal variations of the vertical strain-rate patterns, the

Raymond Effect. So far the occurrence of this effect in-situ has principally been determined indirectly through the analysis of radar layers. By precisely measuring the differential displacement of internal radar reflectors, the phase-sensitive radar (pRES) [*Corr et al.*, 2002; *Jenkins et al.*, 2006] allows a direct measurement of the Raymond Effect with sufficient resolution and accuracy to characterise the ice rheology at natural strain-rates.

[4]   Here, we present pRES data obtained along four transects crossing ice ridges on the Greenland ice sheet. Surface vertical strain-rates are fitted using the results of a full-Stokes numerical model of the Raymond Effect, where the flow along the ridge is taken into account. Finally, we discuss the implications of our estimate of n for the operation of the Raymond Effect, for the ice rheology in-situ and for ice dynamics in general.

2.   Ice Rheology and the Raymond Effect

[5]   The flow law of ice is commonly characterised by Glen's flow law [*Cuffey and Paterson*, 2010], which relates the strain-rate tensor e to the deviatoric stress tensor τ by

$$\tau = 2Be^{1-1/n}e \qquad (1)$$

where B is the temperature dependent stiffness factor, e is the second invariant of the strain-rate tensor and n is the Glen index. Laboratory determination of the rheological parameters of ice have predominantly been at strain-rates higher than those prevailing in natural conditions. Several physical mechanisms for ice deformation compete depending on stress, temperature, crystal size and impurity concentration [*Schulson and Duval*, 2009]. Consequently, a wide range of values for the rheological parameters of ice in ice sheets can be found in the literature. Several attempts have been made to measure the strain-rates and characterise the flow law of ice in-situ: from borehole inclination [e.g., *Dahl-Jensen and Gundestrup*, 1987], bubbly-ice densification [e.g., *Lipenkov et al.*, 1997], or strain sensors in boreholes [e.g., *Elsberg et al.*, 2004; *Pettit et al.*, 2011]. However, no agreement on the rheological parameters can be found, the main difficulty in the field being to properly characterise the stress state. In particular, a value of $n = 3$ is now commonly used in ice flow models, but published values range from 1 to 5.

[6]   Because ice viscosity is non-linearly dependent on the deviatoric stresses, the presence of a highly viscous plug of nearly-stagnant ice is expected just under ice divides or ridges, leading to variation of the vertical strain-rate profile from the ridge to the flank. Owing to this effect [*Raymond*,

[1]Laboratoire de Glaciologie et Géophysique de l'Environnement, UMR 5183, UJF - Grenoble 1, CNRS, Grenoble, France.
[2]Physical Sciences Division, British Antarctic Survey, Natural Environment Research Council, Cambridge, UK.
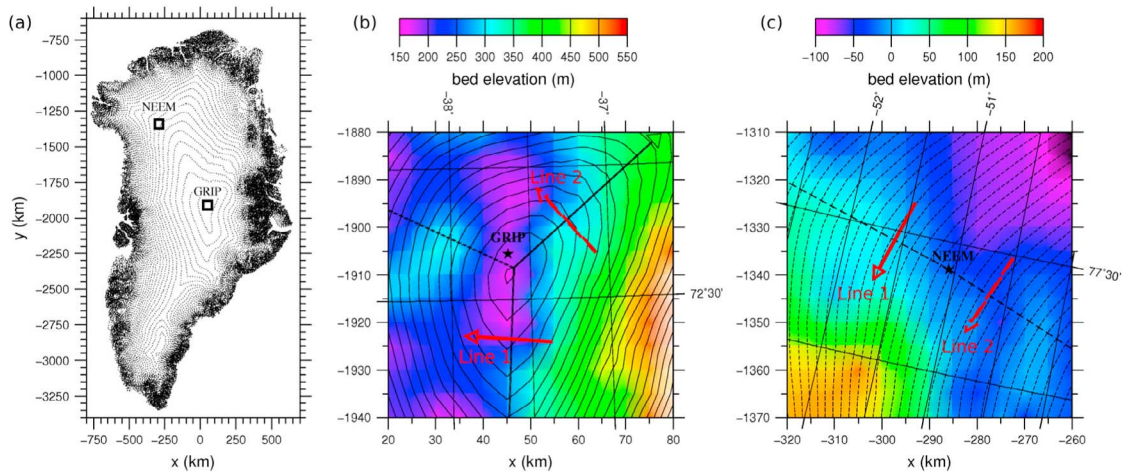
Figure 1. (a) Greenland map showing the NEEM and GRIP areas localisation. (b) Surface contours (every 2.5 m) and bed topography in the Summit area. Black arrows indicate estimated direction of the ridges. (c) Surface contours (every 5 m) and bed topography in the NEEM area. Black dashed line indicate estimates of the ridge direction. At each site, the two red lines are the two lines surveyed with the radar (straight arrow for Line 1 and dashed arrow for Line 2). Maps are based on 5 km DEMs [*Bamber et al.*, 2001].

1983], isochronic surfaces are expected to drape over the plug producing 'Raymond arches', which have been frequently observed in radargrams [e.g., *Conway et al.*, 1999; *Vaughan et al.*, 1999; *Hindmarsh et al.*, 2011]. The size and the shape of these arches depend not only on the ice rheology [*Pettit and Waddington*, 2003; *Martín et al.*, 2006], but also on the ice-flow history [*Nereson et al.*, 1998], and thus provide only indirect measurements of the Raymond Effect. Some surface strain-rate measurements [*Hvidberg et al.*, 2001] and vertical strain-rate measurements from strain-sensors in boreholes [*Pettit et al.*, 2011] indicate differences in strain-rates between divides and flanks that are consistent with the Raymond Effect, but do not have sufficient accuracy or resolution to determine n.

[7] Provided we can measure variations of the vertical strain-rate across an ice divide predicted by the Raymond Effect with sufficient resolution, we can confirm that this is a sufficiently strong influence to cause the formation of Raymond arches. We can further expect to be able to infer the Glen-exponent n *in-situ* by comparing with the stress state obtained from ice flow modelling.

3. Experimental Design

[8] Our phase-sensitive radar has been deployed in the area of the topographic dome of Greenland and near the new deep ice core project NEEM to measure the *in-situ* strain-rates (Figure 1). Two lines centered on the estimated divide position were surveyed at each site. Each line consist of 33 points of measurement, is 18 km long and is centered on the estimated divide position. For more details see section 1 of Text S1 in the auxiliary material.[1]

[9] Our equipment consisted of a network analyzer (PNA E8356A) configured as a step frequency radar housed in a temperature-controlled case sitting on a sledge. Identical broadband aerials were positioned on the snow and

___
[1]Auxiliary materials are available in the HTML. doi:10.1029/2011GL049843.

separated by 8 m. They were operated at a center frequency of 314 MHz and a bandwidth of 142 MHz, using 7095 uniformly spaced frequency steps. The instrument was calibrated before each measurement by connecting the transmit and receive aerials. Since both phase and amplitude of the signal were recorded, changes in the reflector position can be measured to a small fraction of the wavelength [*Jenkins et al.*, 2006]. Measurements were repeated after intervals of one year using the same set-up and taking care to reposition precisely the equipment with respect to the bamboo markers left in place.

[10] The frequency-domain signal is converted to the complex time-domain [*Corr et al.*, 2002], and then to an equivalent depth in ice, taking the speed of radar waves in solid ice to be 168 m μs^{-1}. The firn is left out of the analysis. Figure 2a shows a typical radar record of the amplitude against depth from NEEM Line 2. Beneath the direct breakthrough from the transmitter, amplitude falls to the noise floor at around 1000 m in this case. Zooms of amplitude and phase from two measurements taken one year apart are given in Figures 2b and 2c.

[11] Good reflectors exhibit a relatively high amplitude and a constant phase within them [*Jenkins et al.*, 2006]. Stable reflectors exhibiting a good cross correlation of the amplitude and phase between the two measurements are selected and the mean phase difference is computed over the reflector width. Assuming the reflectors to be material surfaces, the phase difference between the two sets of measurements is proportional to the motion of ice, having accounted for the possibility of uncertainty in the integer number of wavelengths. As we only require differences to compute the strain-rates, the displacement was set to a datum of zero for a good reflector at around 100 m depth, beneath the firn layer. The displacement is converted to an equivalent velocity in ice using the time between the two measurements and the velocity of the waves in solid ice. This procedure typically leads to ten vertical velocity measurements per 100 m of ice.
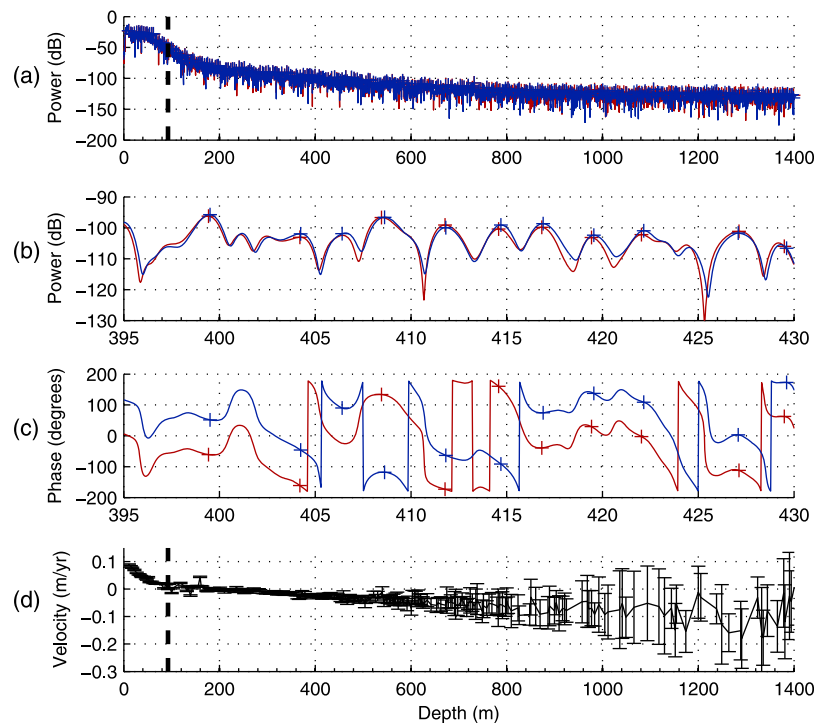
Figure 2. Plot as a function of the equivalent depth in ice for point 11 of Line 2 at NEEM of (a) received power, (b and c) zoom of the received power and phase and (d) ice vertical velocity and error inferred from phase difference. Measurements taken in July 2008 in red, July 2009 in blue. Ice velocity set to nominal zero at reference depth (indicated by the dashed line in top and bottom plots).

[12] The velocity profile measured at this point are plotted on Figure 2d. The large velocity gradient between 0 and 100 m is due to snow compaction. Below, from 100 m to 180 m, where the returned power decreases rapidly (Figure 2a), the amplitude and phase of the two sets of measurements are less stable, leading to some noise in the velocity profile. Below this (Figures 2b and 2c) the shape of both amplitude and phase are very similar, leading to a smooth derived velocity profile down to about 800 m depth, with increased variation lower down arising from the disappearance of the reflectors within the noise.

[13] The instrument error for each reflector is estimated from the amplitude of the reflector compared with the noise level. The phase error for each reflector takes into account a constant error of 3° for the procedure of selecting the reflectors and computing their mean phase difference. We obtain a relatively small error in the vertical velocity in the upper part of the ice-sheet, which increases with depth as reflector strength fades (Figure 2d).

[14] The velocity profile between 200 m and the depth where the reflectors disappear in the noise is fitted by a linear function of depth using a weighted least-squares method, allowing us to estimate the error in the strain-rate measurement. Additional quadratic terms are not found to be statistically significant, following the methodology of *Jenkins et al.* [2006]. This is in agreement with model results that show that the vertical strain-rates are nearly uniform in the upper parts of the ice sheet [e.g., *Martín et al.*, 2006].

[15] Since velocity error increases with depth, the linear fit is largely determined by the upper points. The uniform vertical strain-rate, the gradient of the velocity profile, reflects the vertical strain-rate at the surface. The smooth velocity profile and the relatively small velocity errors on these upper points leads to a small uncertainty for the derived surface strain-rates, between 1 and 5×10^{-5} yr^{-1}. Surface vertical strain-rates and their uncertainty obtained at Summit and NEEM are given on Figures 3a–3c.

[16] For the two lines at NEEM, vertical strain-rates do not show significant variation across the divide. In the Summit area, vertical surface strain-rates are greater in magnitude beneath the divide and they are larger under the South divide. The strain-rates also exhibit an asymmetry with respect to the divide.

4. Numerical Modelling and Fitting Procedure

[17] We use Elmer/Ice to model the flow of ice. As true 3D full-Stokes modelling is still too expensive to be easily used in an inverse procedure to fit the data [*Gillet-Chaulet and Hindmarsh*, 2011], we use a simpler 2.5D model where we assume that the flow along the divide is non-zero but periodic and parameterized by the along-ridge slope γ (section 2 of Text S1). The stiffness parameter B in equation (1) varies with depth according to the GRIP temperature profile [*Gundestrup et al.*, 1993]. Results obtained with this model with $n = 3$ for three different values of γ are given in Figures 3d–3f. As in the 2.5D model of *Martín et al.* [2009b], when γ increases, the velocity along the divide increases. As a consequence, the Raymond Effect, which implies higher absolute vertical strain-rates at the divide compared with the flank, is muted by the along-ridge flow and the maximum thinning rate under the divide decreases as γ increases. In consequence, the surface slope perpendicular to the divide shows stronger variations in the divide area
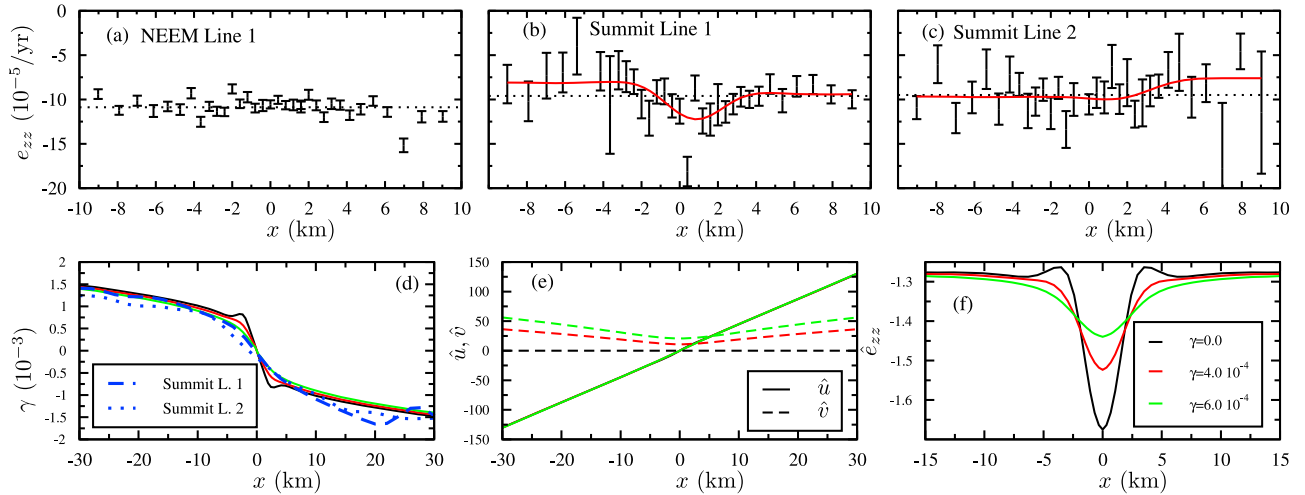
Figure 3. (top) Experimental results: Vertical strain-rates and 1-σ errors for (a) NEEM Line 2, (b and c) Summit Line 1 and Line 2. Dotted lines are the mean values. The x-axis increases in direction indicated by arrows in Figure 1. NEEM Line 1 values were inaccurate owing to instrument problems. Shown in red for Summit Lines are best fits for rheological modelling. (bottom) Numerical results of the 2.5D model with Glen index $n = 3$. Shown, plotted as function of distance from divide, x, are (d) the slope transverse to the ridge, (e) the horizontal velocity transverse to the ridge ($\hat{u}$, solid lines) and along the ridge ($\hat{v}$, dashed lines), normalized with respect to the accumulation. The $\hat{u}$ lines are superimposed. (f) the vertical strain-rates $\hat{e}_{zz}$, normalized with respect to the accumulation over the ice thickness at the dome. Black lines are for along ridge slopes $\gamma = 0$, red lines for $\gamma = 4 \times 10^{-4}$ and green lines for $\gamma = 6 \times 10^{-4}$. The two blue curves in Figure 3d are the observed slopes transverse to ridge derived from the 5 km DEM along Summit Lines 1 (dashed line) and 2 (dotted line).

when γ is low. The variation of the flow velocity perpendicular to the divide is identical for the three experiments. In Figure 3d, the slopes are compared with the slopes along the radar Lines 1 and 2 at Summit given by a 5km DEM [*Bamber et al.*, 2001]. The slope along the divide where Line 1 crosses is 4×10^{-4} and for Line 2 it is 6×10^{-4}. There is good agreement between the surface slopes given by the model and surface slopes along the survey lines derived from the DEM.

[18] To fit the strain-rates data obtained at Summit, we write the objective cost function

$$J = \frac{1}{2}(e_{zz} - \tilde{e}_{zz})C_{ee}(e_{zz} - \tilde{e}_{zz}) + \lambda(e_{zz} - f(x - x_d; n, a_\ell, a_r, \gamma)) \quad (2)$$

where $\tilde{e}_{zz}$ are the observed strain rates; C_{ee} is the error covariance matrix of the strain-rate data, it is diagonal and derived directly from the strain-rate error estimates; e_{zz} are the strain rates estimated at the measurement points; the strain-rates $f(x - x_d; n, a_\ell, a_r, \gamma)$ are based on the 2.5D full-Stokes model results and have four unknown parameters: the Glen index n, the accumulation rates on either side of the divide a_ℓ, a_r, and the divide offset x_d, i.e., the offset between the estimated topographical divide position and the location of the minimum of the vertical strain-rate. The Lagrange multiplier λ constrains the estimated strain-rates e_{zz} to being solutions of the flow model f.

[19] Best estimate of the four unknowns parameters that minimize J in equation (2) are given in Table 1 and best fits to the Summit strain-rate data are plotted in Figure 3. More details on the choice of f and the minimization procedure can be found in section 3 of Text S1.

[20] The fitting procedure used here takes into account only the measurement errors, leading to rather small errors

for the best fit parameters that do not reflect the true sources of uncertainty. The errors on the stress state inferred from ice flow modelling are more difficult to estimate; the main model assumptions are discussed in details in section 4 of Text S1. Plausible errors in the along-ridge slope give rise to an estimate of n lying between 4.3 and 4.8, while 3D effect and uncertainties in the ice activation energy have a small effect. Numerical results with an anisotropic flow law show a reduction of the Raymond effect with a non-zero along-ridge slope but confirm the influence of the ice rheology towards the base.

5. Discussions and Conclusions

[21] The uniform pattern of surface vertical strain-rates in the NEEM area (Figure 3a) shows that the Raymond Effect is not operating, being muted by the flow along the divide. This is predicted by numerical simulations and also shows that there is no special accumulation pattern immediately at the divide. The results obtained at Summit show horizontal variations of the strain-rate associated with an operating Raymond Effect. This is the first *direct* confirmation of the operation of the Raymond Effect from surface measurements, rather than inferring its operation from radar layer geometry.

Table 1. Best Fit Parameters Investigated for Summit Lines 1 and 2[a]

	n	a_l (m/yr)	a_r (m/yr)	x_d (km)
Summit Line 1	4.5	0.22	0.26	0.62
Summit Line 2	4.9	0.27	0.21	1.74

[a]Glen index, n, accumulation on the left, a_l, and on the right, a_r, of the divide, and divide offset, x_d.

[22] Our results confirm that the fact that Raymond arches are not seen in the radargrams in an area where the Raymond effect is operating means that the divide has not been in a stable position long enough for the arches to form over the appropriate advection timescale [*Marshall and Cuffey*, 2000]. Not only can we exclude non-operation of the Raymond Effect arising from a (quasi-)linear ice flow law, but we can also state that the higher absolute strain-rates we measured over the divide indicate that wind scouring at the divide (where absolute strain-rates would be lower) is not an explanation for the formation of Raymond arches. The values of accumulation inferred from optimal fitting are for a steady state divide. The different values deduced from best fit on each side of the divide (a_l and a_r in Table 1) either mean that there is a different pattern on each side of the divide, possibly associated with wind deposition, or that divide migration is giving rise to different strain-rates.

[23] We have used our results to characterise the ice rheology. Assuming ice follows the Glen flow law implies a high value of n around 4.5. Such high values have also been reported from the study of Raymond arch amplitude [*Martín et al.*, 2006]. Anisotropy does not seem to be an explanation as, in our 2.5D model calculations, it reduces the Raymond Effect by enhancing the shearing horizontal plane component along the ridge (see section 4 of Text S1). Nevertheless, in agreement with *Pettit et al.* [2007] and *Martín et al.* [2009a], the Raymond Effect is sensitive to the fabric profile in the lowest part of the ice-sheet. Below 2800 m at GRIP, the temperature is above $-10°C$ and the micro-stuctures are characteristic of dynamic recrystallisation [*De La Chapelle et al.*, 1998]. Dynamic recrystallisation is usually associated with a non-steady or a tertiary creep regime for which values of $n = 4$ have been reported [*Schulson and Duval*, 2009]. Thus, our value could be characteristic of this regime as, for grounded ice, most of the deformation is concentrated near the bed.

[24] Regarding the variations of temperature, microstructure, impurities content and strain-rates with depth, several physical mechanisms are certainly competing to accommodate the deformation and our results cannot be held to contradict the low value of the stress exponent expected for cold ice at low deviatoric stresses. This could explain why the usual $n = 3$ value gives better results when investigations aim at matching the surface profile of the ice-sheet as in that of *Gillet-Chaulet and Hindmarsh* [2011]. Owing to the low strain-rates measured, over the one year time-interval used, the signal to noise ratio is relatively low, giving only a measurement of the vertical strain-rates in the upper 30% of the ice-sheet.

[25] Our results challenge the isotropic Glen flow law with $n = 3$ used in most ice sheet models. Laboratory studies of ice rheology evidently do not provide a full description of *in-situ* ice rheology. It is worth noting that pure metals have stress exponents of 4.5 [*Weertman*, 1999], but we offer no explanation as to why this should be appropriate for ice flow at divides. Our results have direct implications for precise flow modelling around cores at divide or dome positions. They support the non-linear velocity profiles used for dating Dome C and Dome Fuji ice cores [*Parrenin et al.*, 2007]. Furthermore, we need to establish their general applicability, since a high value of n can have significant consequences for grounding line retreat [*Schoof*, 2007] and transient response of ice-streams to downstream perturbation

[*Hindmarsh*, 2006]. Thus, more efforts are needed to constrain *in-situ* ice rheology in polar ice sheets. Systems such as pRES, which can take closely-spaced measurements of vertical strain-rates, are useful tools to achieve this goal.

References

Bamber, J. L., R. L. Layberry, and S. P. Gogineni (2001), A new ice thickness and bed data set for the Greenland ice sheet: 1. Measurement, data reduction, and errors, *J. Geophys. Res.*, *106*, 33,773–33,780.

Conway, H., B. Hall, G. Denton, A. Gades, and E. Waddington (1999), Past and future grounding-line retreat of the West Antarctic ice sheet, *Science*, *286*, 280–283.

Cuffey, K. M., and W. S. B. Paterson (2010), *The Physics of Glaciers*, 4th ed., Academic, Amsterdam.

Corr, H. F. J., A. Jenkins, K. W. Nicholls, and C. S. M. Doake (2002), Precise measurement of changes in ice-shelf thickness by phase-sensitive radar to determine basal melt rates, *Geophys. Res. Lett.*, *29*(8), 1232, doi:10.1029/2001GL014618.

Dahl-Jensen, D., and N. Gundestrup (1987), Constitutive properties of ice at Dye 3, Greenland, in *The Physical Science Basis of Ice Sheet Modelling*, edited by E. D. Waddington and J. S. Walder, *IAHS Publ.*, *170*, 31–43.

De La Chapelle, S., O. Castelnau, V. Lipenkov, and P. Duval (1998), Dynamic recrystallization and texture development in ice as revealed by the study of deep ice cores in Antarctica and Greenland, *J. Geophys. Res.*, *103*, 5091–5105.

Elsberg, D. H., et al. (2004), Depth- and time-dependent vertical strain rates at Siple Dome, Antarctica, *J. Glaciol.*, *50*, 511–521.

Gillet-Chaulet, F., and R. C. A. Hindmarsh (2011), Flow at ice-divide triple junctions: 1. Three-dimensional full-Stokes modeling, *J. Geophys. Res.*, *116*, F02023, doi:10.1029/2009JF001611.

Gundestrup, N. S., D. Dahl-Jensen, S. J. Johnsen, and A. Rossi (1993), Bore-hole survey at dome GRIP 1991, *Cold Reg. Sci. Technol.*, *21*, 399–402.

Hindmarsh, R. C. A. (2006), The role of membrane-like stresses in determining the stability and sensitivity of the Antarctic ice-sheets: Back-pressure and grounding line motion, *Philos. Trans. R. Soc. A*, *364*, 1733–1767, doi:10.1098/rsta.2006.1797

Hindmarsh, R. C. A., E. C. King, R. Mulvaney, H. F. J. Corr, G. Hiess, and F. Gillet-Chaulet (2011), Flow at ice-divide triple junctions: 2. Three-dimensional views of isochrone architecture from ice-penetrating radar surveys, *J. Geophys. Res.*, *116*, F02024, doi:10.1029/2009JF001622.

Hvidberg, C. S., K. Keller, N. Gundestrup, and P. Jonsson (2001), Ice divide flow at Hans Tausen Iskappe, north Greenland, from surface movement data, *J. Glaciol.*, *47*, 78–84.

Jenkins, A., H. F. J. Corr, K. W. Nicholls, C. L. Stewart, and C. S. M. Doake (2006), Interaction between ice and ocean observed with phase-sensitive radar near an Antarctic ice-shelf grounding line, *J. Glaciol.*, *52*, 325–346.

Lipenkov, V. Y., A. N. Salamatin, and P. Duval (1997), Bubbly-ice densification in ice sheets: II. Applications, *J. Glaciol.*, *43*, 397–407.

Marshall, S. J., and K. M. Cuffey (2000), Peregrinations of the Greenland Ice Sheet divide in the last glacial cycle: Implications for central Greenland ice core, *Earth Planet. Sci. Lett.*, *179*, 73–90.

Martín, C., R. C. A. Hindmarsh, and F. J. Navarro (2006), Dating ice flow change near the flow divide at Roosevelt Island, Antarctica, by using a thermomechanical model to predict radar stratigraphy, *J. Geophys. Res.*, *111*, F01011, doi:10.1029/2005JF000326.

Martín, C., G. H. Gudmundsson, H. D. Pritchard, and O. Gagliardini (2009a), On the effects of anisotropic rheology on ice flow, internal structure, and the age-depth relationship at ice divides, *J. Geophys. Res.*, *114*, F04001, doi:10.1029/2008JF001204.

Martín, C., R. C. A. Hindmarsh, and F. J. Navarro (2009b), On the effects of divide migration, along-ridge flow, and basal sliding on isochrones near an ice divide, *J. Geophys. Res.*, *114*, F02006, doi:10.1029/2008JF001025.

Nereson, N. A., C. F. Raymond, E. D. Waddington and R. W. Jacobel (1998), Migration of the Siple Dome ice divide, West Antarctica, *J. Glaciol.*, *44*, 643–652.

Parrenin, F., et al. (2007), 1-D-ice flow modelling at Epica Dome C and Dome Fuji, East Antarctica, *Clim. Past*, *3*, 243–259.

Pettit, E. C., and E. D. Waddington (2003), Ice flow at low deviatoric stress, *J. Glaciol.*, *49*, 359–369.

Pettit, E. C., T. Thorsteinsson, H. P. Jacobson, and E. D. Waddington (2007), The role of crystal fabric in flow near an ice divide, *J. Glaciol.*, *53*, 277–288.

Pettit, E. C., et al. (2011), The crossover stress, anisotropy and the ice flow law at Siple Dome, West Antarctica, *J. Glaciol.*, *57*, 39–52.

Raymond, C. F. (1983), Deformation in the vicinity of ice divides, *J. Glaciol.*, *29*, 357–373.

Schoof, C. (2007), Ice sheet grounding line dynamics: Steady states, stability, and hysteresis, *J. Geophys. Res.*, *112*, F03S28, doi:10.1029/2006JF000664.

Schulson, E. M., and P. Duval (2009), *Creep and Fracture of Ice*, Cambridge Univ. Press, Cambridge, U. K.

Vaughan, D. G., H. F. J. Corr, C. S. M. Doake, and E. D. Waddington (1999), Distortion of isochronous layers in ice revealed by ground-penetrating radar, *Nature*, *398*, 323–326.

Weertman, J. (1999), Microstructural mechanisms in creep, in *Mechanics and Materials: Fundamentals and Linkages*, edited by M. A. Meyers, R. W. Armstrong, and H. Kirchner, 613 pp., John Wiley, New York.

H. F. J. Corr, R. C. A. Hindmarsh, A. Jenkins, and E. C. King, Physical Sciences Division, British Antarctic Survey, Natural Environment Research Council, High Cross, Madingley Road, Cambridge CB3 0ET, UK. (hfjc@bas.ac.uk; rcah@bas.ac.uk; ajen@bas.ac.uk; ecki@bas.ac.uk)

F. Gillet-Chaulet, Laboratoire de Glaciologie et Géophysique de l'Environnement, UMR 5183, UJF - Grenoble 1, CNRS, 54 rue Molière, BP 96, F-38041 Grenoble CEDEX, France. (gillet-chaulet@lgge.obs.ujf-grenoble.fr)